EVIDENCE FOR A CORRELATION BETWEEN ASTROPHYSICAL NEUTRINOS AND RADIO FLARES

YJAN A. GORDON¹, PETER S. FERGUSON², ERIC J. HOOPER³, AND MICHAEL N. MARTINEZ¹

¹Department of Physics, University of Wisconsin-Madison, 1150 University Ave, Madison, WI 53706, USA

²Department of Astronomy, University of Washington, 3910 15th Avenue NE, Seattle, WA 98195, USA

³Department of Astronomy, University of Wisconsin-Madison, 475 N. Charter Street, Madison, WI 53703, USA

Version November 27, 2025

Abstract

We use data from the first two epochs of the Very Large Array Sky Survey (VLASS) and the IceCube Neutrino Observatory to search for evidence of a correlation between radio variability and the detection of astrophysical neutrinos. We find an excess number of associations between flaring radio sources and neutrinos that were detected between the first and second VLASS observations at $> 2\sigma$ confidence. This excess is consistent with radio flares contributing $\sim 13\,\%$ of the astrophysical neutrinos observed by IceCube. Notably $> 80\,\%$ of the radio flares associated with neutrinos are not detected at either γ -ray or X-ray wavelengths, highlighting the importance of radio observations for identifying potential electromagnetic counterparts to astrophysical neutrinos. No excess in the number of associations between the wider radio-variable population and the IceCube neutrinos is seen when no time constraint is placed on the neutrino detection. We predict that data from future VLASS epochs will see an excess number of associations between radio flares and neutrinos at the $> 3\sigma$ level, and expected improvements to the positional constraints on the neutrinos may increase that confidence to $> 5\sigma$, should our results be representative.

Subject headings: Active galactic nuclei (16), Blazars (164), Extragalactic radio sources (508), Neutrino Astronomy (1100), Radio Astronomy (1338), Time Domain Astronomy (2109)

1. INTRODUCTION

Astrophysical neutrinos present a unique way to study the cosmos. Their low interaction cross section allows them to pass through highly dense environments that are opaque to electromagnetic radiation (particularly at shorter wavelengths). Moreover, the extremely low probability of interaction means that neutrinos can reach Earth from the farthest and earliest reaches of the Universe—unlike light, neutrinos have no effective horizon. In recent years, the IceCube Neutrino Observatory has confirmed the existence of high energy (HE; $E_{\nu} \gtrsim 1 \,\mathrm{TeV}$) astrophysical neutrinos (IceCube Collaboration 2013). Some of these HE neutrinos are diffuse emission from the plane of the Milky Way (Icecube Collaboration et al. 2023), potentially resulting from cosmic rays in the Milky Way's interstellar medium. Further to this, two extragalactic point sources of HE neutrinos have been identified so far: the blazar TXS 0506 + 065. and the Seyfert galaxy NGC 1068 (IceCube Collaboration et al. 2018, 2022). Active galactic Nuclei (AGN) such as TXS 0506 + 065 and NGC 1068 are intriguing candidates as neutrino sources, with their central engine's potentially hosting a number of mechanisms that should in theory produce HE neutrinos, e.g., magnetic reconnection events in the accretion disk halo, or shocks in the jet or accretion disk (Mannheim 1995; Bednarek & Protheroe 1999; Khiali & de Gouveia Dal Pino 2016; Blandford et al. 2019; Murase & Stecker 2023). However, with only a handful of neutrino sources identified to date, it is difficult to determine what processes are responsible for the HE astrophysical neutrinos we observe. The relativistic outflows and radiative processes found in a variety of energetic astronomical phenomena may result in the particle acceleration necessary for HE neutrino production. Consequently, events such as gamma-ray bursts (GRBs), supernovae (SNe), and tidal disruption events (TDEs) provide theoretical alternative sources for observed HE neutrinos (Razzaque et al. 2003; Denton & Tamborra 2018; Morgan et al. 2019; Stein et al. 2021; Winter 2024).

Identifying electromagnetic counterparts to neutrino detections has proven difficult. Any one HE neutrino detection has a relatively small chance of being a real astrophysical neutrino. Moreover, the typically large positional uncertainties for neutrino detections encompass many potential sources of origin. A representative circular positional error for an IceCube detection has a radius of $\sim 1^{\circ}$ (Aartsen et al. 2017a) covering an area of $\sim 3 \deg^2$. Modern deep optical surveys typically detect hundreds of thousands of sources per square degree; for example, the on-sky source density, ρ , of the Hyper Suprime Cam wide survey is $\sim 270,000 \, \mathrm{deg}^{-2}$ (Aihara et al. 2022). It is therefore usually not possible to confidently associate a single neutrino detection with an electromagnetic counterpart. As a result, observational studies of the origins of astrophysical neutrinos typically rely on one of two approaches. First, associations of multiple neutrino events with a single point of origin increase the likelihood that the source in question is a neutrino emitter. This is the approach that led to TXS 0506 + 056 and NGC 1068 being identified as neutrino-producing AGN (IceCube Collaboration et al. 2018, 2022). Second, socalled stacking experiments that combine large numbers of low-probability associations in order to identify trends in whether certain source types are more often associated with neutrinos than would be expected from random matching of two unrelated populations. This latter approach cross correlates multiple neutrino detections with multiple objects of a given type, e.g., star-forming galaxies or blazars (Bechtol et al. 2017; Aartsen et al. 2017b; Fang et al. 2020; Abbasi et al. 2024).

The production mechanism for neutrinos invariably results in high energy electromagnetic radiation. Consequently, incorporating time-domain information into searches for the electromagnetic counterparts to HE neutrinos can reduce uncertainty in the associations between individual neutrino events and potential sources of origin. For instance, neutrinos have been observed at similar times to γ -ray, X-ray and radio outbursts in blazars that are spatially coincident with the neutrino detection (e.g., Kadler et al. 2016; The KM3NeT Collaboration et al. 2025). Stacking experiments that search for correlations between electromagnetic flares and HE neutrinos have had shown some intriguing results. For example, Hovatta et al. (2021) and Kouch et al. (2024) find a potential correlation between radio outbursts in the blazar population and HE neutrinos at the $\sim 2\sigma$ level; Lu et al. (2025) identified a likely correlation between optical flares associated with TDEs and HE neutrinos at $\sim 2.5 \,\sigma$ confidence; while van Velzen et al. (2024) report a $3.6\,\sigma$ confidence association between HE neutrinos and what they term "accretion flares" (a superset of optical outbursts in AGN and TDEs), using a combination of optical and infrared observations.

Radio observations are a particularly promising avenue in the search for electromagnetic counterparts to HE astrophysical neutrinos for three key reasons. First, many of the phenomena thought to produce HE neutrinos (AGN, SNe, GRBs, and TDEs) are expected to emit radio waves. Indeed, the two confirmed neutrino point sources to date are both bright at radio frequencies (e.g., Kuehr et al. 1981; Laurent-Muehleisen et al. 1997). Second, the long wavelengths of radio are less subject to scattering than shorter wavelength observations (e.g., γ rays). Consequently radio observations can probe the dense environments of theorized neutrino producers that will likely be opaque to the HE photons also produced (Murase et al. 2016; Murase 2022). Third, radio sources often have higher redshifts than objects not detected in the radio, and thus sample a larger volume of the Universe (Gordon et al. 2025). As such, for neutrinos originating at high redshift, the radio emission (if produced) may be bright enough to be detected when the source is too faint to (currently) be observed at other wavelengths, potentially increasing the number of neutrinos for which an electromagnetic counterpart is detected.

The advent in recent years of deep and wide-area time-domain radio sky surveys, such as the Karl G. Jansky Very Large Array Sky Survey (VLASS, Lacy et al. 2020) and the Variables And Slow Transients survey (VAST, Murphy et al. 2013), opens up new possibilities in searching for electromagnetic counterparts to HE neutrinos (Perger et al. 2024, 2025; Filipović et al. 2025). Previously, searches for correlations between radio variability and HE neutrino detections have been limited to bright sources with radio flux densities, S, typically brighter than a few hundred mJy. In contrast, the latest generation of radio surveys can detect variability in objects

that are orders of magnitude fainter, with $S\gtrsim$ a few mJy (Gordon et al. 2025), detecting potential neutrino counterparts that are intrinsically less luminous and/or across a larger cosmic volume. To that end, in this work we search for evidence of a correlation between variable radio sources detected in VLASS and HE neutrinos detected by IceCube.

The rest of this paper is laid out as follows. Section 2 describes the VLASS and IceCube data used in this work. In Section 3 we describe the process of associating variable radio sources with neutrino events and details of the statistical analysis we perform on the identified radio-neutrino associations. We discuss our results along with future prospects in Section 4, and a summary of this work is given in Section 5.

2. DATA 2.1. *VLASS*

The Karl G. Jansky Very Large Array Sky Survey (VLASS, Lacy et al. 2020), is a multi-epoch survey of the entire sky north of $\delta = -40^{\circ}$ at $\nu \sim 3\,\mathrm{GHz}$ that began in 2017. The survey has a synthesized beam size of $\sim 3''$ and a typical rms noise of $130\,\mu\mathrm{Jy}$ beam⁻¹ in each epoch, making VLASS the highest resolution, deep, nearall-sky radio continuum survey to date. Approximately 1.8×10^6 sources brighter than $\sim 1\,\mathrm{mJy}$ are detected in a VLASS epoch (Gordon et al. 2021), with $\sim 2.5\,\mathrm{years}$ between VLASS epochs. To date, three VLASS epochs have been observed, a fourth epoch began observing in September 2025 (Nyland et al. 2023), with full catalogs available for the first two epochs at the time of writing.

We identified 3,618 variable radio sources in Gordon et al. (2025) based on Epoch 1 (September 2017 - July 2019) and Epoch 2 (June 2020 - February 2022) of VLASS. The majority of these sources were found to be probable blazars, and using the data from Gordon et al. (2025) not only allows us to know where they are on the sky but also provides a window when we know some of these sources experienced outbursts of activity. In Gordon et al. (2025) our aim was to characterize the variable radio population, and we were able to do this for sources varying in flux density by 30% or more across the two epochs. Here we are specifically looking for more substantive changes in brightness and select only those variables exhibiting at least a 50% change in flux density. Explicitly, we select the 1,928 sources with |m| > 0.4 for use in this work, where $m = \Delta S/\overline{S}$ is the modulation index for a source with flux density measurements S (see also Section 3.3 and Table 1 in Gordon et al. 2025). These objects have mean brightnesses, $\mu_S = (S_{\text{Epoch 1}} + S_{\text{Epoch 2}})/2$, in the range 1 mJy $\lesssim \mu_S \lesssim$ 1 Jy with a median value of $\mu_{S, P50} \approx 14$ mJy. Our data therefore samples a substantially fainter population than previous works that are typically limited to the radio variables in dedicated monitoring programs, generally brighter than a few hundred mJy (e.g., Hovatta et al. 2021; Kouch et al. 2024). We perform no cuts to the radio sample on source type—we don't, for example, specifically select stars or galaxies based on multiwavelength data. The advantage of such a source-agnostic selection is that we don't eliminate potential neutrino sources, with one of the major objectives of this work being to assess the efficacy of using faint radio time-domain sky surveys in identifying electromagnetic counterparts to astrophysical neutrinos.

2.2. IceCube

The IceCube Observatory (Aartsen et al. 2013; IceCube Collaboration 2013) detects Cherenkov radiation caused by charged leptons produced during the interactions of high energy neutrinos with the Antarctic ice. Since 2012, IceCube detects $\sim 3,000$ muons a second, the vast majority of which are from cosmic rays (Aartsen et al. 2016). Real astrophysical neutrinos are thought to account for around 30 events per year in the IceCube data, and discrete tracks created by their interaction with the ice can be traced to an on-sky point of origin. The typical angular precision of such tracks is on the order of 1°, depending on factors such as the neutrino energy and track length (Aartsen et al. 2017a).

To search for neutrino detections potentially associated with variable sources, we make use of the IceCat-1 catalog (Abbasi et al. 2023). IceCat-1 lists track-like events detected by IceCube since 2011 that are considered likely to have an astrophysical origin. Typically these have a signal $\gtrsim 0.3$, where the signal is ostensibly a probability of being a real astrophysical neutrino that is based on the modeled neutrino energy and likely declination of origin. Some of the events recorded in IceCat-1 have signal < 0.3; these are very high energy events $(E_{\nu} > 100 \, \text{TeV})$ that are identified either as targets for follow up gamma-ray observations, or as a result of having extremely high energies ($E_{\nu} > 500 \, \text{TeV}$; for full details we refer the reader to Section 2 of Abbasi et al. 2023). In this work, we use version 2 of IceCat-1¹, which lists 348 IceCube track events up until October 2023. In Figure 1 we show how the on-sky origins of the neutrinos (red circles) are distributed relative to the coordinates of the variable VLASS sources (blue dots). It is worth noting that there is a strong declination selection effect in the IceCat-1 catalog where neutrinos are easier to detect at equatorial and lower northern declinations.

3. CROSS ASSOCIATION OF VLASS VARIABLES WITH ICECAT-1

3.1. Associating Radio Sources with Neutrino Events

In order to assess if a correlation exists between radio sources and HE neutrinos, we must first identify which neutrinos could be associated with which radio sources. The radio source positions in the sky are very well constrained, having a typical astrometric precision on the order of a few tenths of an arcsecond (Gordon et al. 2021). The neutrino source positions have much poorer constraints, typically having positional uncertainties on the order of a degree (Aartsen et al. 2017a). IceCat-1 provides positive and negative 90% confidence limits on the R.A. and Decl. of the neutrino detections. We use these uncertainties to define error ellipses in which we expect the radio counterpart (should there be one) to lie, and consider any of our VLASS sources within this ellipse to be a spatially associated candidate for the neutrino source (e.g., see Figure 2). In addition to this spatial association, the availability of flux densities from

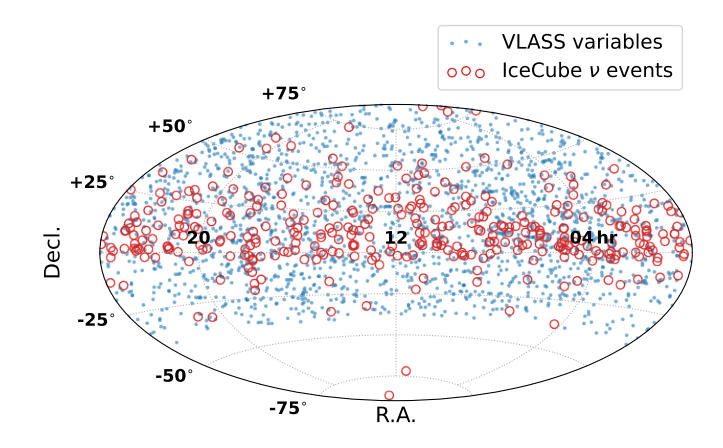


Fig. 1.— The on-sky distribution of VLASS variables (blue dots) and IceCube neutrino events from IceCat-1 (red circles) used in this work shown on an Aitoff projection in equatorial coordinates. Note that the size of the red circles is arbitrary and does not correspond to the positional uncertainty of the neutrinos.

two VLASS epochs allows us to ascertain if there is any temporal association between the neutrino event and the radio variability. For instance, if a neutrino is associated with a radio flare, one might expect its observation date to be correlated with the increase in radio brightness of the source. We consider a VLASS source to be temporally associated with a neutrino if the neutrino was detected in a time window defined by the observation dates of the first and second VLASS epochs.

We define three samples of VLASS variables with which to search for a correlation with HE neutrinos. One is the full sample of 1,928 variables, for which we search for a spatial association only. This allows us to search for any variable radio sources that may have produced neutrinos in an outburst prior to the variability captured by VLASS between epochs 1 and 2, and we refer to this sample as the 'full variable sample' throughout the rest of this work. The second sample is the subset of 1,093 radio variables that brightened between VLASS Epoch 1 and Epoch 2. These objects are known to have experienced an outburst of activity between the two VLASS epochs. We search for sources that have a spatial association and temporal association such that the time the neutrino was detected, t_{ν} , lies between the observation times for VLASS Epoch 1, $t_{\rm VLASS~1}$, and VLASS Epoch 2, $t_{\text{VLASS 2}}$, i.e., $t_{\text{VLASS 1}} < t_{\nu} < t_{\text{VLASS 2}}$. We will refer to this sample as the *flaring sample* throughout the rest of this work. The third sample consists of the same 1,093 radio sources as in the flaring sample, but for the temporal correlation we shift the time window in which we allow the neutrino to be associated. The reasoning behind this is that in blazars—one of the principle theorized sources of origin for HE astrophysical neutrinos—radio outbursts can lag behind γ -ray flares by \sim a few hundred days (Max-Moerbeck et al. 2014). Given that the neutrino production will result in γ -ray emission, one might expect the radio flare to also be delayed relative to the neutrino event. Max-Moerbeck et al. (2014) found that 150 days was the median lag between γ -ray and radio flares in blazars when such a time lag was detected with high confidence. To account for this we shift the time window in which we look for a neutrino association by 150 days for our third sample, achieved in practice by

 $^{^1}$ https://dataverse.harvard.edu/dataset.xhtml?persistentId=doi:10.7910/DVN/SCRUCD

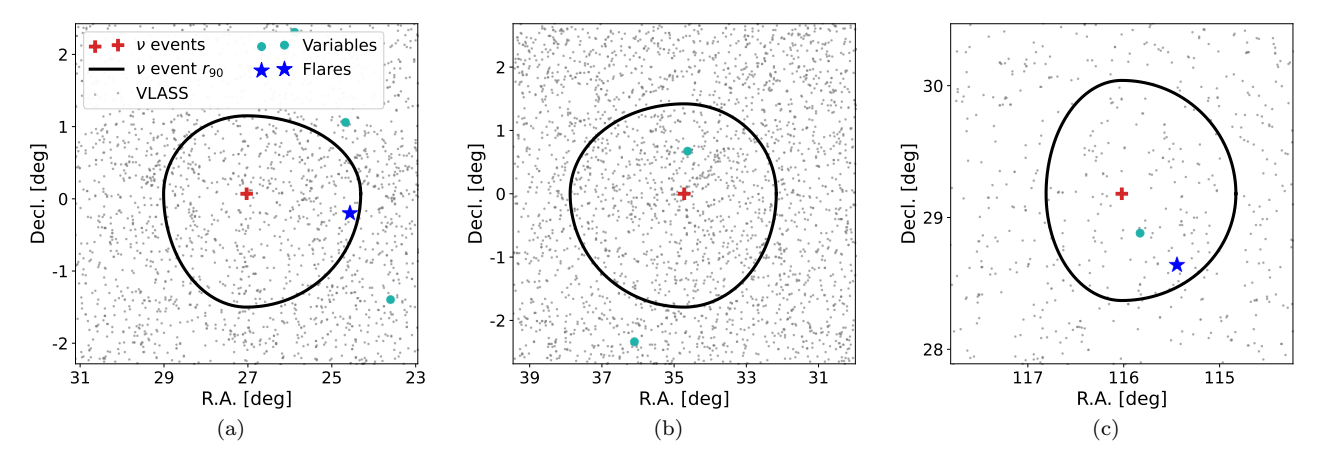


FIG. 2.— Example IceCube events consistent with VLASS sources. In all panels the red cross shows the most likely origin coordinates of the neutrino, the black ellipse shows the 90 % positional confidence, gray dots show VLASS sources, light green circles are variable VLASS sources, and blue stars highlight flares in VLASS that are consistent with the neutrino event time. Note that the apparent relative sparsity of VLASS sources in panel (c) is an effect of the panel being zoomed in on a neutrino event with a smaller positional uncertainty than in panels (a) and (b).

TABLE 1
RADIO TEST SAMPLES USED IN THIS WORK

Sample Name (1)	$N_{ m radio}$ (2)	$t_{ u}$ (3)
Full variables Flaring Lagged-flaring	1,928 1,093 1,093	any $t_{\rm VLASS~1} < t_{\nu} < t_{\rm VLASS~2}$ $t_{\rm VLASS~1} < t_{\nu} + 150{\rm days} < t_{\rm VLASS~2}$

NOTE. — The name of the test sample (1); the number of radio sources in the sample (2), the neutrino event time, t_{ν} , required in order to be associated with this sample.

adding 150 days to the neutrino's event time in IceCat-1, i.e., $t_{\rm VLASS~1} < t_{\nu} + 150\,{\rm days} < t_{\rm VLASS~2}$. That is to say a neutrino event detected 150 days prior to the Epoch 1 VLASS observation would be considered associated with the radio flare, but an event detected 149 days prior to the Epoch 2 observation would not. For the rest of this work we will refer to this third sample as the lagged-flaring sample. We list these three samples, their sizes, and the temporal association we consider in Table 1.

We match all three samples of VLASS variables to the IceCat-1 data. For the full variable sample using only a spatial association we find 446 associations with IceCat-1, consisting of 381 radio sources consistent with 138 neutrino events. When considering radio flares that are spatially and temporally associated with neutrinos, the flaring sample has 64 associations with IceCat-1, 63 radio sources and 28 neutrino events; and the lagged-flaring sample has 62 associations, 62 radio sources and 27 neutrino events. As might be expected given the relatively long cadence of VLASS, there is substantial overlap between the two time correlated sets, with 59 radio sources and 24 neutrinos appearing in both samples. In the flaring sample there are 4 radio sources and 4 neutrinos that aren't in the lagged flaring sample, while in the laggedflaring sample there are 3 radio sources and 3 neutrino events that do not appear in the flaring sample.

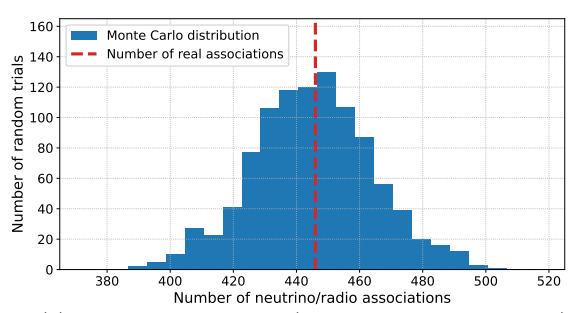
It is important to note that using our definitions of associations can result in multiple candidate radio counterparts for a single neutrino event (e.g., see Figure 2c).

This is to be expected when considering the large uncertainties in the neutrino position, and the on-sky density of sources in VLASS. For instance, the the median radius of the 90% confidence positional uncertainty in the IceCat-1 data is $\sim 80'$, corresponding to a typical on-sky footprint of $\sim 5.6\,\mathrm{deg}^2$ in which the neutrino's source origin is expected to lie. VLASS has a source density of $\rho \sim 53 \, \mathrm{deg}^{-2}$, so a typical neutrino detection is expected to have ~ 300 candidate counterparts in VLASS. Radio sources that vary by > 50% in flux density are far rarer, with our data here having a typical on-sky source density of $\rho \sim 0.06\,\mathrm{deg^{-2}}$, corresponding to an average of 0.3 of these objects expected to be associated with any given IceCat-1 detection. For those neutrinos where there are multiple associated radio sources, only one of these, if any, can be the true point of origin of the neutrino. It is also possible for some radio sources to be associated with multiple neutrino events—especially when there is no time constraint required for the association. Such sources are of interest on their own as multiple neutrino associations with an object reduce the likelihood of the associations being coincidental. We will study these candidate multi-neutrino radio variables in depth in a future work. Our aim in this paper is not to identify the correct source of origin of neutrino events, but rather to look for potential trends in whether variable radio sources as population might be consistent with neutrinos more often than would be expected if those associations were due to random chance.

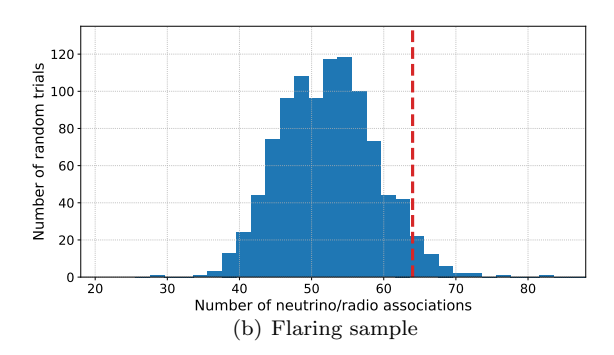
3.2. Comparisons with the Expected Random Background Contribution

3.2.1. Numbers of Associations

In order to test whether the observed numbers of associations between variable radio sources and HE neutrinos are significant, we perform a 1,000 iteration Monte Carlo simulation for each test sample. In each iteration, N random sky coordinates within the VLASS footprint are used to simulate the radio population, where N is the number of radio sources in the real test sample (e.g., N=1,928 for the full variable sample). In practice these simulated sky positions are achieved by random-



(a) Full variables sample (positional association only)



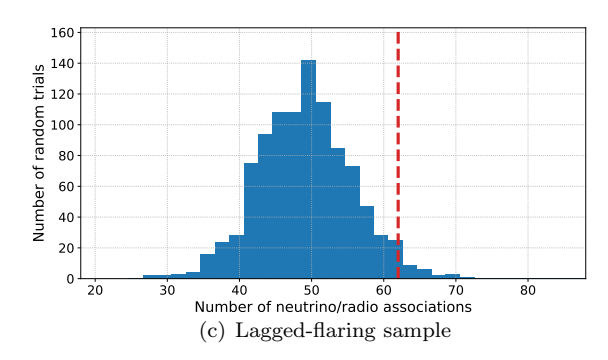


FIG. 3.— The number of associations between VLASS radio sources and IceCube neutrinos for our three test samples. In each panel the blue histogram shows the distribution of the association count in the 1000 run Monte Carlo simulation, and the red dashed line shows the observed number of associations.

izing the list of R.A. coordinates for the radio source test sample, an approach that ensures the simulated radio sources have the same declination distribution as the real radio sources. As the VLASS footprint is simply defined as $\delta > -40^{\circ}$, retaining the declination distribution of the real radio samples will result in simulated positions that are also within the VLASS footprint. Moreover, maintaining the radio source declination distribution mitigates the potential for the declination bias of the IceCat-1 events (the clustering of red circles toward the equator in Figure 1) to impact our comparisons of real and simulated radio-neutrino associations. Shuffling the R.A. of the radio sources also has the secondary effect of randomizing the time-domain information for the two samples where we are also searching for evidence of a temporal correlation. Any real temporal correlation with the neutrinos that may exist will be lost in the mock data as the sky positions will be random, allowing the Monte

TABLE 2
Observed and expected counts for radio-neutrino associations, radio sources, and neutrino events.

Sample Name		N	$\mu \pm \sigma$	$p ext{-value}$		
(1)		(2)	(3)	(4)		
Radio-Neutrino Associations						
Full variables		446	445 ± 19	0.471		
Flaring		64	52 ± 7	0.034		
Lagged-flaring		62	49 ± 6	0.021		
Radio Sources						
Full variables		381	384 ± 15	0.572		
Flaring		63	51 ± 6	0.031		
Lagged-flaring		62	48 ± 6	0.019		
Neutrino Events						
Full variables		138	147 ± 7	0.769		
Flaring		28	26 ± 3	0.260		
Lagged-flaring		27	23 ± 3	0.144		
Flaring Lagged-flaring Full variables Flaring		381 63 62 Events 138 28	51 ± 6 48 ± 6 147 ± 7 26 ± 3	0 0 0		

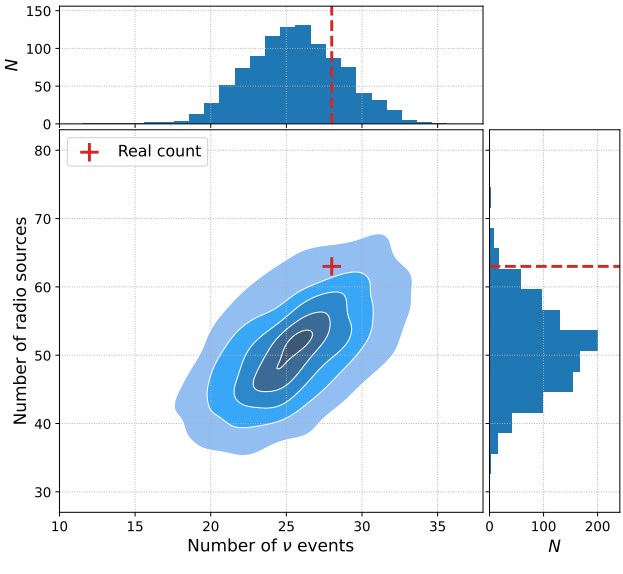
Note. — The radio sample used in the test (1); the observed count (2); the expected mean and standard deviation from the Monte Carlo simulation (3); and the p-value of the observed count (4).

Carlo to effectively simulate a random background of flaring sources for the flaring and lagged-flaring samples.

In Figure 3 we show histograms of the number of associations between radio sources and neutrinos from the Monte Carlo simulations for each of the three test samples. On each panel, the real observed number of associations is shown by a dashed red vertical line. Any real correlation should show an excess number of associations relative to random background, and the significance of any excess can be estimated as a p-value defined by the fraction of simulations with more associations than the observed value. The Monte Carlo simulation of the full variable sample (Figure 3a) has mean and standard deviation of 445 ± 19 associations, consistent with the observed value of 446 associations. Of the 1,000 iterations, 471 resulted in \geq 446 associations, suggesting a p-value of 0.471 for the observed number of associations in the full variable sample. Both the flaring and lagged flaring samples (panels b and c, respectively of Figure 3) show an elevated number of real associations with the IceCat-1 data compared to the expectation values from the simulated random backgrounds. Assuming no correlation, the expected number of associations for the flaring sample is 52 ± 7 . The real value of 64 associations has p = 0.034 based on the simulated distribution. Similarly, the expected number of associations for the laggedflaring sample is 49 ± 6 , compared to the observed value of 62 with p = 0.021. These statistics are summarized in Table 2, and while not definitive, are suggestive of a correlation between radio flares and neutrino detections at $> 2 \sigma$ confidence.

3.2.2. Radio and Neutrino Counts

In Figure 4, we split the associations into the number of neutrino events and number of flaring radio sources and plot the individual distributions of these counts for the



(a) Flaring sample

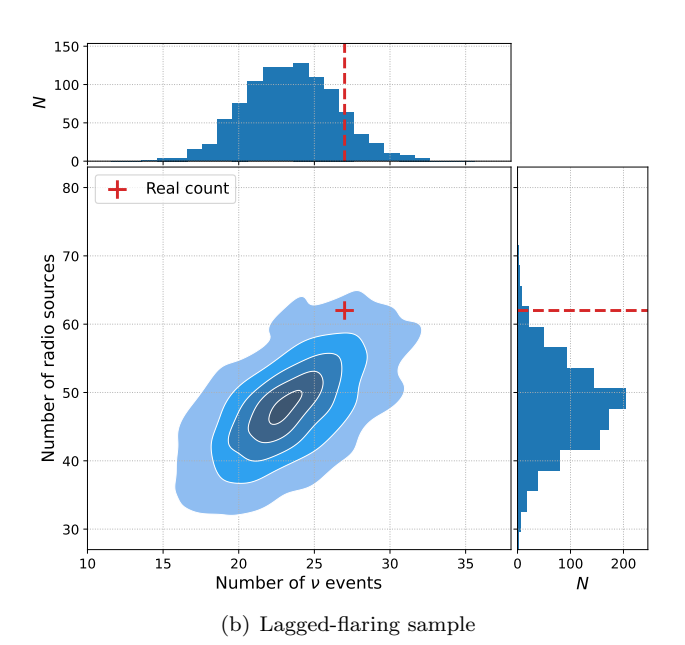


FIG. 4.— The expected background distributions of radio source and neutrino event counts for the two test samples with a higher than expected number of radio-neutrino associations. Panel (a) shows the flaring sample, and panel (b) shows the lagged-flaring sample. In both panels the contours show the 95th, 75th, 50th, 25th, and 5th percentile from the PDF estimated by the Monte Carlo simulation. The red cross and dashed lines show the position of the real numbers of neutrino events and radio sources associated.

two test samples where we see a higher than expected number of radio-neutrino associations. We observe 63 radio sources associated with 28 neutrinos in the flaring sample. From the Monte Carlo simulation we would expect 51 ± 6 radio sources and 26 ± 3 neutrino events, with estimated p-values for the real counts of 0.031 and 0.260, respectively. For the lagged-flaring sample, 62 radio sources are associated with 27 neutrino events. The mean (\pm the standard deviation) and p-values in the associated Monte Carlo simulation are 48 ± 6 with p=0.019 for the radio source counts, and 23 ± 3 with p=0.144

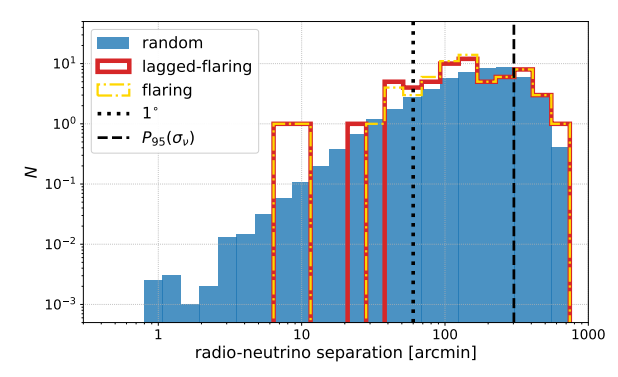


Fig. 5.— Distributions of angular separations between associated radio sources and neutrino events. The solid blue histogram shows random associations from Monte Carlo simulations. Angular separations for real associations from the flaring and lagged-flaring sample are shown by the yellow dot-dashed and red solid lines, respectively. The dashed black vertical line shows the 95th percentile of the positional errors exhibited by IceCat-1 events, σ_{ν} and the dotted black vertical line represents an angle of 1°.

for the neutrino events. These numbers are also summarized in Table 2. The significance of the excess number of associations between radio flares and neutrinos is clearly driven by the number of radio sources rather than the neutrino counts. This is likely due to the rarity of neutrino detections relative to the density of flaring radio sources on the sky.

3.2.3. Angular Separations Between Associations

If there is truly a correlation between variable radio sources and HE neutrinos then one might expect the onsky angular separations between the radio and neutrino detections to be smaller than would be expected from associations that were purely the result of the random background distributions. In Figure 5 we show the distributions of angular separations between the radio source and the neutrino detection for the flaring (yellow dotdashed line) and lagged-flaring (red solid line) samples. The blue histogram in Figure 5 shows the distributions from the Monte Carlo simulations for both the flaring and lagged-flaring samples, weighted by a factor of 1/2000, and thus represents expected number of random associations with a given angular separation. We don't show the distribution for the full variable sample for two reasons. Firstly as there is no evidence for an excess number of associations between this sample and the IceCat-1 events (see Section 3.2.1 and Figure 3a), and secondly so as not to reduce clarity of Figure 5 by overcrowding the plots. The black dotted vertical line represents an angular separation of 1° while the black dashed vertical line shows the 95th percentile of positional uncertainties in IceCat-

The median angular separation for random background associations is 177'. In comparison, the median angular separation for the flaring sample associations is 143', and for the lagged-flaring sample is 139'. Performing KS tests on these distributions returns p-values of p=0.009 and p=0.018 when comparing the flaring and lagged-flaring samples respectively with the expected random background. These statistics suggest that real radio flares are typically closer on the sky to the position of the neutrinos with which they are potentially associated at a

similar confidence level to the observed excess of radioneutrino associations for the flaring and lagged-flaring samples that are presented in Section 3.2.1. While a formalized cross-correlation analysis is beyond the scope of this work, we will investigate the two-point correlation between radio flares and neutrinos in a future paper that uses additional observational data.

4. DISCUSSION

4.1. Multiwavelength Properties of Radio Sources Consistent with Neutrino Events

4.1.1. High Energy Electromagnetic Counterparts

Additional information about flaring radio sources can be gleaned by studying their multiwavelength properties. In Gordon et al. (2025) we obtained for the VLASS variables:

- redshift measurements from the Sloan Digital Sky Survey data release 16 (SDSS DR16, York et al. 2000; Ahumada et al. 2020) and the DESI Legacy Surveys data release 8 (LS DR8, Dey et al. 2019; Duncan 2022);
- infrared counterparts from the Wide-field Infrared Survey Explorer telescope's (WISE, Wright et al. 2010) AllWISE catalog (Cutri et al. 2014);
- and γ-ray counterparts from the fourth Fermi Large Area Telescope data release 4 (4FGL, Abdollahi et al. 2020; Ballet et al. 2023).

Of particular interest here, the mechanisms for neutrino production are also typically expected to produce corresponding high energy photons. We thus might expect flaring radio sources associated with neutrino production to also have a γ -ray counterpart. Taking the union of 66 radio sources in the flaring and lagged flaring samples (59 appearing in both samples, with 7 appearing in only one sample), we find Fermi counterparts to only 4 objects, or 6 % of the sample.

While γ -rays are the most obvious byproduct of neutrino production, their extremely short wavelengths (a 1 GeV photon has a wavelength of $\sim 10^{-5} \,\text{Å}$) make them especially prone to obscuration. The γ -rays produced near the black hole in AGN can be reprocessed into Xray photons (Inoue et al. 2020; Murase et al. 2020), the longer wavelengths of which are less easily obscured. Indeed, there is recent observational evidence of a potential correlation between X-rays at energies of a few tens of keV and neutrinos detected by IceCube (Kun et al. 2024). We therefore also check to see how many of our radio sources have X-ray counterparts. To do this we use version 2 of the Millions of Optical-Radio/X-ray catalog (MORX, Flesch 2024), which includes probabilistic associations between VLASS sources and their likely X-ray counterparts observed by the Chandra X-ray Observatory (Weisskopf et al. 2000, 2002), XMM-Newton (Jansen et al. 2001), the Neil Gehrels Swift Observatory (Burrows et al. 2005), and ROSAT (Truemper 1982). Of the 66 flaring radio sources, just 9 (14%) have an X-ray counterpart in MORX.

It is notable that very few of the associated radio sources have high energy electromagnetic counterparts, even though such short wavelength radiation should be a byproduct of the neutrino production. One possible explanation for this is that the radio sources without γ -ray or X-ray counterparts are merely spurious background associations. A second possibility, as mentioned above, is that the neutrinos are produced in a dense environment resulting in obscuration of the associated high energy photons. A third possibility is that the radio observations are probing a larger cosmic volume (i.e., are sensitive to objects at higher redshifts) than the available γ -ray and X-ray data—we showed in Section 5.3 of Gordon et al. (2025) that VLASS variables with 4FGL counterparts tend to have lower redshifts than those without. The observability of electromagnetic radiation is intrinsically tied to the flux density of that radiation resulting in an observable cosmic horizon. Neutrinos on the other hand only interact via the weak nuclear force and gravity, not via electromagnetism. As such their detection is probabilistic, and subsequently neutrinos have no effective cosmic horizon. Probing larger cosmic volumes in the electromagnetic regime therefore increases the number of opportunities to identify the sources of origin for astrophysical neutrinos. Approximately half of our flaring radio sources (35/66) have a redshift measurement from either SDSS DR16 or LS DR8, with a median redshift of $z_{P50} = 1.04$. Only one of the sources with a γ -ray counterpart has an associated redshift (z=0.76). and 6 of those with X-ray detections have redshifts, with a median value of $z_{P50} = 0.83$. It is of course difficult to draw strong conclusions based on only a handful of objects, but our data are consistent with the idea that the radio flares sample a larger cosmic volume than is currently possible with γ -rays and X-rays. Whether one or more of the possibilities presented here is responsible for the lack of high energy electromagnetic counterparts to the flaring radio sources associated with the IceCat-1 neutrino events, it is clear that our analysis using radio observations allows us to consider sources of origin for the neutrinos that would be missed in analyses limited to short wavelength observations.

4.1.2. Infrared Colors

Radio galaxies are often bright at infrared (IR) wavelengths, and of the 66 flaring radio sources, 56 (85 %) are detected in AllWISE. The IR colors, and in particular the brightness of an object in the three shortest wavelength WISE bands (W1, $3.4 \mu m$; W2, $4.3 \mu m$; and W3, $12 \,\mu\mathrm{m}$), of radio sources can be used to broadly characterize the source hosting the radio emission(e.g., Gürkan et al. 2014; Mingo et al. 2022; Gordon et al. 2023; Wong et al. 2025). In Figure 6, we plot a WISE color-color diagram that shows the W2-W3 color against the W1-W2 color of flaring radio sources. Following the approach in Section 5.2 of Gordon et al. (2025), we only include objects in Figure 6 where the source is detected with at least a signal-to-noise ratio of 2 in all of the three WISE bands, and either has a measured redshift of z < 1 or a brightness of W1 < 14 mag if no redshift is available. Objects at z > 1 tend to move to the right (larger values of W2 - W3) on the WISE color-color diagram as the WISE bands start to trace different regions of the galaxy spectral energy distribution, and thus may no longer be accurately classified according to diagnostic criteria developed for lower redshift galaxies (Donley et al. 2012; Assef et al. 2013). These criteria leave us with 21 flar-

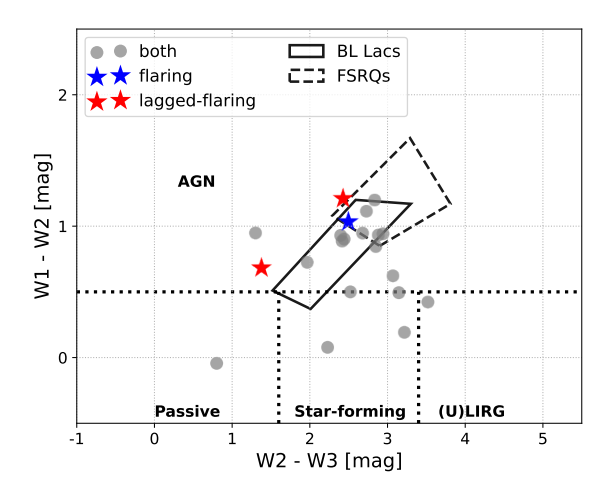


FIG. 6.— WISE color-color diagram for radio flares potentially associated with IceCube neutrino events. Grey circles show sources present in both the flaring and lagged-flaring samples, the one object that only appears in the flaring sample is marked by a blue star, and the two sources that are only in the lagged-flaring sample are shown as red stars. The black dotted lines show the regions occupied by passive galaxies, star-forming galaxies, (ultra) luminous infrared galaxies, and AGN, while the solid and dashed lines show the regions of IR color space where blazars are typically found.

ing radio sources that we show on Figure 6, highlighting those sources that *only* appear in the flaring or lagged-flaring sample as blue and red stars, respectively.

Using the diagnostic criteria of Mingo et al. (2016), we classify the radio source as being hosted by either passive galaxies, star-forming galaxies (SFGs), (ultra) luminous infrared galaxies (ULIRGs), or AGN based on their location on Figure 6. These regions are labeled on the figure and demarcated by dotted black lines. We also show the regions typically occupied specifically by blazars on Figure 6, with the black solid line showing where BL Lacs are found, and the dashed black line highlighting the expected location of flat-spectrum radio quasars (FSRQs). In Table 3 we show the percentage of flaring radio sources associated with each IR population, with uncertainties in these percentages calculated using a binomial approach (Cameron 2011). The percentages for Either Sample in Table 3 include all of the 21 flaring radio sources shown on Figure 6, while the percentages for Both Samples only include the 18 objects that are in both the flaring and lagged-flaring samples. The one source that is in the flaring sample but not in the lagged-flaring sample is a blazar, while the two objects in the lagged-flaring sample but not in the flaring sample both have AGN-like IR colors that are outside the blazar region of the WISE color-color diagram. For reference, we also show the expected percentages in each IR population from the parent sample of radio variables in VLASS taken from Gordon et al. (2025).

For the radio flares associated with IceCat-1 events that have the appropriate WISE data, their IR colors are not significantly different from what we would expect for any radio variable source. This is what we should expect to see given that we have a weak signal for our excess number of radio-neutrino associations, and is perfectly consistent with the associations we do find being dominated by background sources. Of potential note,

TABLE 3
THE IR POPULATION DISTRIBUTIONS OF FLARING RADIO SOURCES
ASSOCIATED WITH NEUTRINO DETECTIONS.

IR Population (1)	Either Sample (2)	Both Samples (3)	Radio Variables (4)
Passive [%]	5^{+9}_{-2} 14^{+11}_{-5} 5^{+9}_{-2} 76^{+7}_{-11}	$6^{+11}_{-2} \\ 17^{+12}_{-5} \\ 6^{+11}_{-2} \\ 72^{+8}_{-12}$	$7^{+2}_{-1} \\ 9^{+2}_{-1} \\ 1^{+1}_{-0} \\ 83 \pm 2$
Blazars [%] BL Lacs [%] FSRQs [%]	$48_{-10}^{+11} \\ 38_{-9}^{+11} \\ 29_{-8}^{+11}$	50 ± 11 39^{+12}_{-10} 28^{+12}_{-8}	68 ± 3 56 ± 3 40 ± 3

NOTE. — IR population based on WISE colors (1) for all radio flares in *either* the flaring or lagged-flaring samples (2), flares in *both* the flaring and lagged flaring samples (3), and the expected proportion of radio variables in each IR population from Gordon et al. (2025, 4).

however, is that the percentage of blazars in our samples of radio flares associated with neutrinos ($\sim 50\,\%$) appears at first glance to be slightly lower than expected for the radio variable population ($\sim 70\,\%$). Similarly the number of SFGs ($\sim 15\,\%$) appears to be slightly higher than we expect from the radio variable population ($\sim 10\,\%$). Neither of these apparent discrepancies is significant, both are at the $\sim 1\sigma$ level. However, should future analyses show a correlation between neutrinos and electromagnetic counterparts at high confidence, then significant differences may start to show between neutrino associated sources and their parent population, which may in turn help us to better understand which types of objects that produce astrophysical neutrinos.

4.2. Contribution of Radio Flares to the High Energy Astrophysical Neutrino Counts

Assuming the excess number of associations between radio flares and neutrino events to be real and representative, we can estimate the contribution of the flaring radio source population to the observed HE astrophysical neutrinos. Let us consider the lagged flaringsample, where we see the highest significance increase in associations between radio sources and neutrinos relative to expectations (p = 0.019). The number of observed associated neutrinos is $N_{\nu,\rm obs}=27$ and the expected number of neutrinos from random background associations is $N_{\nu, \text{bg}} = 23 \pm 3$. The apparent excess number of neutrinos associated with the radio sources is therefore $N_{\nu,\rm ex}=N_{\nu,\rm obs}-N_{\nu,\rm bg}=4\pm3.$ We can compare this to the total expected number of astrophysical neutrinos expected to be detected—whether or not they are associated with a radio source—over the typical time window between radio observations in VLASS. The median time between an Epoch 1 and Epoch 2 observation in VLASS is 974 days (Gordon et al. 2025). The average number of IceCat-1 events between the start of VLASS Epoch 1 and the end of VLASS Epoch 2 was 0.072 per day, or approximately 70 events between VLASS observations. Each event in IceCat-1 has a signal metric that is an estimate of the probability that the event was due to a

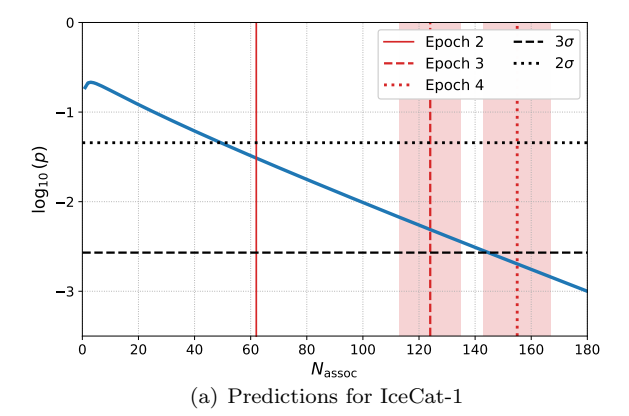
real astrophysical neutrino (e.g., as opposed to an atmospheric source, Abbasi et al. 2023). The mean signal for IceCat-1 events between Epoch 1 and 2 of VLASS was 0.44, implying that of the 70 IceCat-1 events in a 974 day period, 31 should be from an astrophysical source. We would expect the excess number of observed neutrinos associated with radio sources to be drawn from these 31 astrophysical events, suggesting that $13\pm10\,\%$ of astrophysical neutrinos are produced by sources experiencing an observable outburst in radio emission.

While the low significance in the excess number of radio-neutrino associations prevents us from making more firm constraints on the contribution of radio flares to the observed astrophysical neutrino counts, we can compare our estimate to expectations based on previous works. The samples of variable radio sources are selected only on their radio variability properties and are otherwise agnostic to object type. That is to say, we don't differentiate between whether the radio emission comes from a star, galaxy, quasar, or another phenomenon. From Gordon et al. (2025) we expect the dominant population of variable radio sources to be blazars. Previous works have demonstrated that blazars are expected to contribute $\lesssim 10\%$ of the observed neutrino flux (e.g., Padovani et al. 2015; Aartsen et al. 2017b; Murase et al. 2018). In Table 3 we show that $\sim 1/2$ of the flaring radio sources associated with neutrinos have blazar-like IR colors. If the real radio-neutrino associations that may exist in our data are drawn randomly from the IR populations presented in Section 4.1.2, then that could suggest that $\sim 6-7\%$ of astrophysical neutrinos originate from blazars. Notably, this number is similar to finding of Kouch et al. (2025), who estimate that $\lesssim 8\%$ of neutrinos originate from blazars. Given the selection bias toward blazars in the radio-variable population, a contribution of $\sim 13\%$ to the astrophysical neutrino counts by flaring radio sources seems realistic to first order.

4.3. Future Prospects

The variable radio sources used in this work were identified based solely on observations from the first two epochs of VLASS. For the flaring and lagged-flaring samples—where we see some evidence of a correlation with IceCat-1—associations between the radio source and the neutrino are limited to a single ~ 2.5 year window. If the correlation we see evidence for in Section 3.2.1 is in fact real, then observing more such associations between the flares and neutrino events will reduce the shot noise and increase our confidence that a correlation exists. Future IceCube and VLASS data may prove useful here. VLASS Epoch 3 covers the same footprint as Epochs 1 and 2, to the same depth, and at the same cadence. It is thus reasonable to assume that the number of radio flares between Epoch 2 and Epoch 3 will be similar to the number of flares between Epoch 1 and Epoch 2. VLASS Epoch 4 will observe half the footprint of Epochs 1-3, resulting in half as many flares between Epochs 3 and 4 as between Epochs 1 and 2. Assuming a constant average event detection rate at IceCube, the number of associations between VLASS flares and astrophysical neutrinos should scale linearly with the number of flares observed.

We can estimate the significance for a given number of associations between neutrinos and radio flares, $N_{\rm assoc}$



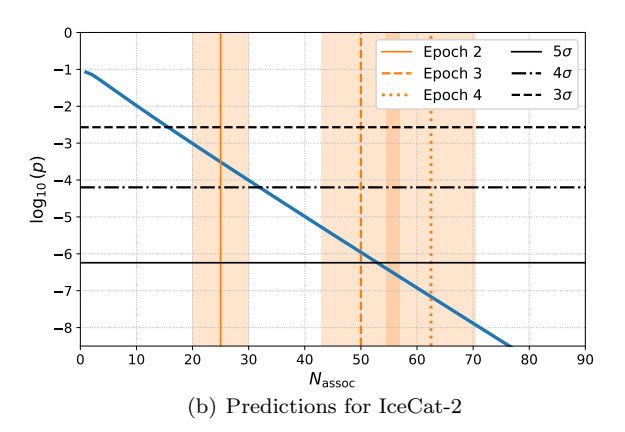


Fig. 7.— Predicted p-value (see Equation 1 in text) for a given number of associations between radio flares and HE neutrinos based on the observations presented in this work and assuming a Poisson distribution. Panel (a) shows the predictions using IceCat1, and panel (b) is an estimate based on the expected improvements to neutrino positional confidence in IceCat-2. In each panel the vertical lines show the expected number of associations at the end of a given VLASS epoch: solid vertical for the end of Epoch 2 (this work in panel a), dashed vertical for the end of Epoch 3, and dotted vertical for the end of Epoch 4. The shaded regions around the vertical lines are the \sqrt{N} uncertainties in the expected counts. The black horizontal lines highlight the p-values corresponding to 2σ (dotted), 3σ (dashed), 4σ (dot-dashed), and 5σ (solid) confidence.

as:
$$p = 1 - F(N_{\text{assoc}}|\lambda), \tag{1}$$

where p is the estimated p-value for a given number of associations, F is the Poisson CDF, and λ is the expected number of associations assuming the null hypothesis of no correlation between the neutrinos and radio flares. In Section 3.2 our lagged-flaring sample showed $N_{\rm assoc}=62$ compared to an expected $\lambda=49$. From this we can estimate that the fraction of associations that are background events as $f_{\rm bg}=\lambda/N_{\rm assoc}=0.79$. In Figure 7a we show the predicted p-value (Equation 1) for increasing numbers of associations between VLASS flares and IceCat-1 neutrinos assuming this value for $f_{\rm bg}$, with the expected number of associations by the end of VLASS Epochs 3 and 4 highlighted by red vertical dashed and dotted lines respectively. If there is actually a correlation between VLASS flares and IceCat-1 neutrinos at the level we see in this work, then we would expect to de-

tect that correlation with $> 3\sigma$ confidence by the end of VLASS Epoch 4.

A future version of IceCat known as IceCat-2 will include improved angular resolution for both new and historical neutrino events (Zegarelli et al. 2025). The positional uncertainties in IceCat-2 are expected to cover $\sim 1/4$ of the solid angle subtended by the IceCat-1 uncertainties, leading to a corresponding reduction in the number of random background associations with electromagnetic counterpart candidates. From our lagged-flaring sample, the number of excess associations over the expected random background can be estimated as $N_{\rm ex} = 62 - 49 = 13$. With the improved IceCat-2 uncertainties we would expect 1/4of the background associations that are observed in IceCat-1, leading to ~ 25 associations $(N_{\rm ex} + \lambda/4)$, with $p = 1 - F(25|12) = 3 \times 10^{-4}$. In panel (b) of Figure 7, we show the expected p-values for increasing numbers of associations between radio flares and neutrinos assuming that the IceCat-2 data does in fact reduce the shot noise as expected. By the end of VLASS Epoch 4 we anticipate $N_{\rm assoc}=62$ and $\lambda=30$ using the IceCat-2 data, an observation that would have $p \sim 10^{-7}$, or $> 5\sigma$ confidence. We obtain a similar prediction when estimating $N_{\rm assoc}$, λ , and $N_{\rm bg}$ using the results from the flaring sample as opposed to the lagged-flaring sample.

5. SUMMARY AND CONCLUSIONS

In this work we investigate whether variable radio sources contribute to the astrophysical neutrinos observed by IceCube. Radio-variable objects are widely considered to be likely candidate neutrino sources but until recently such research has generally been limited to the brightest and most well-studied variable radio sources. The recent advent of wide-area, deep (flux densities down to a few mJy), time-domain radio surveys like VLASS allow the expansion of radio-neutrino cross-association stacking experiments to include a more complete sampling of the radio-variable population. We use data from the first two epochs of VLASS and the IceCat-1 catalog of neutrino events to perform such an analysis. Our key findings are summarized below.

- We find an excess number of associations between flaring radio sources and neutrinos that are both spatially and temporally associated when compared to the expected number of random associations, at $> 2\sigma$ confidence.
- Radio flares that are spatially and temporally associated with neutrinos are typically located closer

on the sky to the neutrino event than simulated random associations. Real associations have a median angular separation of 140' compared to 180' for random associations. Comparing the distributions these angular separations via a KS test returns a p-value of < 0.02.

- The majority (> 80%) of radio sources associated with IceCat-1 events are not detected at γ-rays or X-rays, highlighting the importance of radio timedomain surveys in identifying candidate electromagnetic counterparts to astrophysical neutrinos.
- \bullet The excess number of neutrinos identified by these associations is consistent with flaring radio sources contributing $\sim13\,\%$ of the astrophysical neutrinos observed by IceCube, in agreement with previous studies.
- The number of associations between variable radio sources and neutrinos is consistent with the expected background when no time correlation is required, i.e., there is no evidence of a spatial-only correlation between radio variables and neutrinos.
- Assuming our results are representative, we predict that the significance of the excess number of associations between radio flares and neutrinos will exceed 3σ confidence by the end of VLASS Epoch 4. Should the improved uncertainties in the sky position of neutrino events in the forthcoming IceCat-2 also lower the shot noise as expected, then we anticipate $> 5\sigma$ confidence in the excess number of associations between radio flares and HE astrophysical neutrinos.

ACKNOWLEDGMENTS

In carrying out this work we made use of the following software packages and tools: AstroPy (Astropy Collaboration et al. 2013, 2018, 2022), Matplotlib (Hunter 2007), NumPy (Harris et al. 2020), and TOPCAT (Taylor 2005).

The VLA is operated by NRAO, a facility of the National Science Foundation operated under cooperative agreement by Associated Universities, Inc.

WISE is a joint project of the University of California, Los Angeles, and the Jet Propulsion Laboratory/California Institute of Technology, and NEO-WISE, which is a project of the Jet Propulsion Laboratory/California Institute of Technology. WISE and NEOWISE are funded by the National Aeronautics and Space Administration.

REFERENCES

Aartsen, M. G., Abbasi, R., Abdou, Y., et al. 2013, Phys. Rev. Lett., 111, 021103, doi: 10.1103/PhysRevLett.111.021103
Aartsen, M. G., Abraham, K., Ackermann, M., et al. 2016, Astroparticle Physics, 78, 1, doi: 10.1016/j.astropartphys.2016.01.006
Aartsen, M. G., Ackermann, M., Adams, J., et al. 2017a, Astroparticle Physics, 92, 30, doi: 10.1016/j.astropartphys.2017.05.002
Aartsen, M. G., Abraham, K., Ackermann, M., et al. 2017b, ApJ, 835, 45, doi: 10.3847/1538-4357/835/1/45
Abbasi, R., Ackermann, M., Adams, J., et al. 2023, ApJS, 269, 25, doi: 10.3847/1538-4365/acfa95

—. 2024, ApJ, 973, 97, doi: 10.3847/1538-4357/ad643d Abdollahi, S., Acero, F., Ackermann, M., et al. 2020, ApJS, 247, 33, doi: 10.3847/1538-4365/ab6bcb Ahumada, R., Allende Prieto, C., Almeida, A., et al. 2020, ApJS, 249, 3, doi: 10.3847/1538-4365/ab929e Aihara, H., AlSayyad, Y., Ando, M., et al. 2022, PASJ, 74, 247, doi: 10.1093/pasj/psab122 Assef, R. J., Stern, D., Kochanek, C. S., et al. 2013, ApJ, 772, 26, doi: 10.1088/0004-637X/772/1/26 Astropy Collaboration, Robitaille, T. P., Tollerud, E. J., et al. 2013, A&A, 558, A33, doi: 10.1051/0004-6361/201322068 Astropy Collaboration, Price-Whelan, A. M., Sipőcz, B. M., et al. 2018, AJ, 156, 123, doi: 10.3847/1538-3881/aabc4f Astropy Collaboration, Price-Whelan, A. M., Lim, P. L., et al. 2022, ApJ, 935, 167, doi: 10.3847/1538-4357/ac7c74
Ballet, J., Bruel, P., Burnett, T. H., Lott, B., & The Fermi-LAT collaboration. 2023, arXiv e-prints, arXiv:2307.12546, doi: 10.48550/arXiv.2307.12546
Bechtol, K., Ahlers, M., Di Mauro, M., Ajello, M., & Vandenbroucke, J. 2017, ApJ, 836, 47, doi: 10.3847/1538-4357/836/1/47
Bednarek, W., & Protheroe, R. J. 1999, MNRAS, 302, 373, doi: 10.1046/j.1365-8711.1999.02132.x
Blandford, R., Meier, D., & Readhead, A. 2019, ARA&A, 57, 467, doi: 10.1146/annurev-astro-081817-051948
Burrows, D. N., Hill, J. E., Nousek, J. A., et al. 2005, Space Sci. Rev., 120, 165, doi: 10.1007/s11214-005-5097-2
Cameron, E. 2011, PASA, 28, 128, doi: 10.1071/AS10046
Cutri, R. M., Wright, E. L., Conrow, T., et al. 2014, VizieR
Online Data Catalog: II/328. Originally published in: VizieR On-line Data Catalog: II/328. Originally published in: IPAC/Caltech (2013)
Denton, P. B., & Tamborra, I. 2018, ApJ, 855, 37, doi: 10.3847/1538-4357/aaab4a
Dey, A., Schlegel, D. J., Lang, D., et al. 2019, AJ, 157, 168, doi: 10.3847/1538-3881/ab089d
Donley, J. L., Koekemoer, A. M., Brusa, M., et al. 2012, ApJ, 748, 142, doi: 10.1088/0004-637X/748/2/142
Duncan, K. J. 2022, MNRAS, 512, 3662, doi: 10.1093/mnras/stac608
Fang, K., Banerjee, A., Charles, E., & Omori, Y. 2020, ApJ, 894, 112, doi: 10.3847/1538-4357/ab8561
Filipović, M. D., Smeaton, Z. J., Bradley, A. C., et al. 2025, ApJ, 984, L52, doi: 10.3847/2041-8213/adca37
Flesch, E. W. 2024, The Open Journal of Astrophysics, 7, 6, VizieR On-line Data Catalog: II/328. Originally published in: Flesch, E. W. 2024, The Open Journal of Astrophysics, 7, 6, doi: 10.21105/astro.2308.01507 doi: 10.21105/astro.2308.01507
Gordon, Y. A., Ferguson, P. S., Martinez, M. N., & Hooper, E. J. 2025, arXiv e-prints, arXiv:2508.00976, doi: 10.48550/arXiv.2508.00976
Gordon, Y. A., Boyce, M. M., O'Dea, C. P., et al. 2021, ApJS, 255, 30, doi: 10.3847/1538-4365/ac05c0
Gordon, Y. A., Rudnick, L., Andernach, H., et al. 2023, ApJS, 267, 37, doi: 10.3847/1538-4365/acda30
Gürkan, G., Hardcastle, M. J., & Jarvis, M. J. 2014, MNRAS, 438, 1149, doi: 10.1093/mnras/stt2264
Harris, C. R., Millman, K. J., van der Walt, S. J., et al. 2020, Nature, 585, 357, doi: 10.1038/s41586-020-2649-2
Hovatta, T., Lindfors, E., Kiehlmann, S., et al. 2021, A&A, 650, A83, doi: 10.1051/0004-6361/202039481 A83, doi: 10.1051/0004-6361/202039481 Hunter, J. D. 2007, Computing in Science and Engineering, 9, 90, doi: 10.1109/MCSE.2007.55 IceCube Collaboration. 2013, Science, 342, 1242856, doi: 10.1126/science.1242856 IceCube Collaboration, Aartsen, M. G., Ackermann, M., et al. 2018, Science, 361, 147, doi: 10.1126/science.aat2890
IceCube Collaboration, Abbasi, R., Ackermann, M., et al. 2022, Science, 378, 538, doi: 10.1126/science.abg3395
Icecube Collaboration, Abbasi, R., Ackermann, M., et al. 2022.
Science, 380, 1338, doi: 10.1126/science.abg3395
Icecube Collaboration, Abbasi, R., Ackermann, M., et al. 2023,
Science, 380, 1338, doi: 10.1126/science.adc9818
Inoue, Y., Khangulyan, D., & Doi, A. 2020, ApJ, 891, L33,
doi: 10.3847/2041-8213/ab7661
Jansen, F., Lumb, D., Altieri, B., et al. 2001, A&A, 365, L1,
doi: 10.1051/0004-6361:20000036 Kadler, M., Krauß, F., Mannheim, K., et al. 2016, Nature Physics, 12, 807, doi: 10.1038/nphys3715
 Khiali, B., & de Gouveia Dal Pino, E. M. 2016, MNRAS, 455, 2021. 838, doi: 10.1093/mnras/stv2337 Kouch, P. M., Hovatta, T., Lindfors, E., et al. 2025, arXiv e-prints, arXiv:2510.16585, doi: 10.48550/arXiv.2510.16585 Kouch, P. M., Lindfors, E., Hovatta, T., et al. 2024, A&A, 690, A111, doi: 10.1051/0004-6361/202347624 Kuehr, H., Witzel, A., Pauliny-Toth, I. I. K., & Nauber, U. 1981,

This paper was built using the Open Journal of Astrophysics LATEX template. The OJA is a journal which

Kun, E., Bartos, I., Tjus, J. B., et al. 2024, Phys. Rev. D, 110, 123014, doi: 10.1103/PhysRevD.110.123014

A&AS, 45, 367

Lacy, M., Baum, S. A., Chandler, C. J., et al. 2020, PASP, 132, 035001, doi: 10.1088/1538-3873/ab63eb
Laurent-Muehleisen, S. A., Kollgaard, R. I., Ryan, P. J., et al. 1997, A&AS, 122, 235, doi: 10.1051/aas:1997331
Lu, M.-X., Liang, Y.-F., Wang, X.-G., & Ouyang, X.-R. 2025, ApJ, 990, 18, doi: 10.3847/1538-4357/adef54
Mannheim, K. 1995, Astroparticle Physics, 3, 295, doi: 10.1016/0927.6505/04/09044 Mannheim, K. 1995, Astroparticle Physics, 3, 295, doi: 10.1016/0927-6505(94)00044-4

Max-Moerbeck, W., Hovatta, T., Richards, J. L., et al. 2014, MNRAS, 445, 428, doi: 10.1093/mnras/stu1749

Mingo, B., Watson, M. G., Rosen, S. R., et al. 2016, MNRAS, 462, 2631, doi: 10.1093/mnras/stw1826

Mingo, B., Croston, J. H., Best, P. N., et al. 2022, MNRAS, 511, 3250, doi: 10.1093/mnras/stac140 Morgan, R., Bechtol, K., Kessler, R., et al. 2019, ApJ, 883, 125, doi: 10.3847/1538-4357/ab3a45Murase, K. 2022, ApJ, 941, L17, doi: 10.3847/2041-8213/aca53c Murase, K., Guetta, D., & Ahlers, M. 2016, Phys. Rev. Lett., 116, 071101, doi: 10.1103/PhysRevLett.116.071101

Murase, K., Kimura, S. S., & Mészáros, P. 2020, Phys. Rev. Lett., 125, 011101, doi: 10.1103/PhysRevLett.125.011101

Murase, K., Oikonomou, F., & Petropoulou, M. 2018, ApJ, 865, 124, doi: 10.3487/1538.4257/acado00 124, doi: 10.3847/1538-4357/aada00 Murase, K., & Stecker, F. W. 2023, in The Encyclopedia of Cosmology. Set 2: Frontiers in Cosmology. Volume 2: Neutrino Physics and Astrophysics, ed. F. W. Stecker, 483–540, doi: 10.1142/9789811282645_0010 Murphy, T., Chatterjee, S., Kaplan, D. L., et al. 2013, PASA, 30, e006, doi: 10.1017/pasa.2012.006 Nyland, K., Alexander, K., Andernach, H., et al. 2023, VLASS Epoch 4 Science Case, https: //science.nrao.edu/vlass/library/vlass-epoch-4-science-case Padovani, P., Petropoulou, M., Giommi, P., & Resconi, E. 2015, MNRAS, 452, 1877, doi: 10.1093/mnras/stv1467 Perger, K., Frey, S., Gabányi, K. É., & Kun, E. 2024, RNAAS, 8, 44, doi: 10.3847/2515-5172/ad25ea 2025, A&A, 698, L2, doi: 10.1051/0004-6361/202555177
 Razzaque, S., Mészáros, P., & Waxman, E. 2003, Phys. Rev. D, 68, 083001, doi: 10.1103/PhysRevD.68.083001 Stein, R., van Velzen, S., Kowalski, M., et al. 2021, Nature Astronomy, 5, 510, doi: 10.1038/s41550-020-01295-8

Taylor, M. B. 2005, in Astronomical Society of the Pacific Conference Series, Vol. 347, Astronomical Data Analysis Software and Systems XIV, ed. P. Shopbell, M. Britton, & R. Ebert, 29 The KM3NeT Collaboration, MessMapp Group, Fermi-LAT Collaboration, et al. 2025, arXiv e-prints, arXiv:2502.08484, doi: 10.48550/arXiv.2502.08484 Truemper, J. 1982, Advances in Space Research, 2, 241, doi: 10.1016/0273-1177(82)90070-9 doi: 10.1016/0273-1177(82)90070-9
van Velzen, S., Stein, R., Gilfanov, M., et al. 2024, MNRAS, 529, 2559, doi: 10.1093/mnras/stae610
Weisskopf, M. C., Brinkman, B., Canizares, C., et al. 2002, PASP, 114, 1, doi: 10.1086/338108
Weisskopf, M. C., Tananbaum, H. D., Van Speybroeck, L. P., & O'Dell, S. L. 2000, in Society of Photo-Optical Instrumentation Engineers (SPIE) Conference Series, Vol. 4012, X-Ray Optics, Instruments, and Missions III, ed. J. E. Truemper & B. Aschenbach, 2–16, doi: 10.1117/12.391545
Winter, W. 2024, arXiv e-prints, arXiv:2402.19314, doi: 10.48550/arXiv.2402.19314 doi: 10.48550/arXiv.2402.19314 Wong, O. I., Garon, A. F., Alger, M. J., et al. 2025, MNRAS, 536, 3488, doi: 10.1093/mnras/stae2790
Wright, E. L., Eisenhardt, P. R. M., Mainzer, A. K., et al. 2010, AJ, 140, 1868, doi: 10.1088/0004-6256/140/6/1868 York, D. G., Adelman, J., Anderson, Jr., J. E., et al. 2000, AJ, 120, 1579, doi: 10.1086/301513

Zegarelli, A., Franckowiak, A., Sommani, G., Valtonen-Mattila, N., & Yuan, T. 2025, arXiv e-prints, arXiv:2507.06176, doi: 10.48550/arXiv.2507.06176

provides fast and easy peer review for new papers in the astro-ph section of the arXiv, making the reviewing process simpler for authors and referees alike. Learn more at http://astro.theoj.org.